ACS APPLIED MATERIALS & INTERFACES

Research Article

www.acsami.org

High-Yield Synthesis of Sub-10 nm Pt Nanotetrahedra with Bare ⟨111⟩ Facets for Efficient Electrocatalytic Applications

Moumita Rana,[†,‡] Manjeet Chhetri,[†,‡] B. Loukya,[∥] Pramod K. Patil,[†] Ranjan Datta,[∥] and Ujjal K. Gautam*[,†]

[†]New Chemistry Unit, [∥]International Centre for Materials Science, Jawaharlal Nehru Centre for Advanced Scientific Research, Bangalore 560064, India

Supporting Information

ABSTRACT: Unlike other shapes, the design of tetrahedral Pt nanocrystals (Pt-NTd), which have the largest number of Pt(111) surface atoms and highest catalytic activities toward the electron transfer reactions, has widely been considered a synthetic challenge due to their thermodynamic instability. Here, we show that, by inducing their nucleation on functionalized carbon, Pt NTds can be obtained with tunable sizes and high yields. The carbon support anchors the nanocrystals early and prevents their oriented attachment leading to nanowire formation. Therein, an *in situ* generated amine is crucial for stabilization of Pt-NTds, which can later be removed to expose the Pt(111) facets for higher catalytic efficiency. The bare nanocrystals exhibit much improved stability and electrocatalytic activity characteristic of Pt(111) toward oxygen reduction reaction (ORR) and methanol and formic acid oxidation reactions. For example, ∼90% of their activity was retained after 5000 potential cycles, while the ORR onset potential was recorded to be very high, 1.01 V vs reversible hydrogen electrode (RHE).

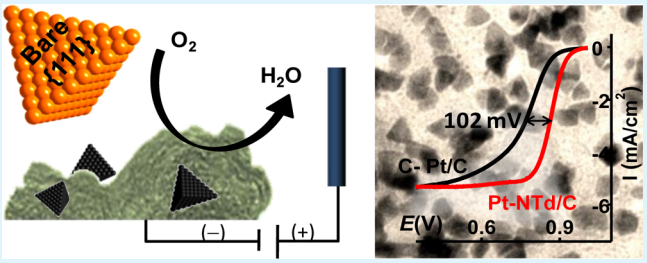

KEYWORDS: *electrocatalysis, Pt(111), metal nanocrystals, oxygen reduction reaction, fuel cell, methanol oxidation*

1. INTRODUCTION

Shape controlled metal nanocrystals have shown great promise for applications in catalysis and renewable energy harvesting.[1−4] Among the different noble metals, nanocrystals (NCs) of Pt are considered as superior catalysts for many commercial processes including various electron transfer reactions, oxidation of fuel molecules, oxygen reduction, and reduction of trans-fat in edibles.[5−10] The efficiency of these catalyst NCs are dependent on their shapes, as different shapes are enclosed with different crystallographic facets.[1,9,11−16] Pt NCs also exhibit higher stability against corrosion in harsh reaction conditions. Interests in improving these efficiencies have inspired the discovery of a large number of synthetic strategies for Pt NCs having different shapes, each with a different set of Pt crystal-facets, atomic arrangements, and reactivity. Those shapes include cubes ({100} planes), octahedra ({111} planes), icosahedra ({111} planes), octapods ({411} planes), and others.[2,17−21] Amidst much progress, however, one aspect has triggered scientific curiosity. As many have observed, Pt NCs with tetrahedral morphology, covered entirely with {111} planes and having the highest number of closed-pack surface atoms, are extremely difficult to prepare. This is particularly the case when the size is less than 20 nm, and instead, thermodynamically more stable Pt octahedral nanocrystals are formed under the experimental conditions.[2,12,22−24] Octahedral NCs also have all {111} surfaces but are more stable than the of tetrahedral Pt nanocrystals (Pt-NTd) due to their smaller surface/edge and the surface/volume ratios. In contrast, other metals as well as alloys of Pt with Ni, Co, or Pd have been found to form tetrahedral NCs rather easily.[12,25,26]

A Pt(111) facet possesses a higher atomic packing density than any other crystal-plane, resulting in lower electron affinity of the exposed Pt atoms. This led to the favorable adsorption of different chemical species, making Pt(111) facet catalytically more efficient than the other ones.[27,28] Besides, these also exhibit the highest stability against leaching and surface corrosion due to the strong cohesive energy (defined as the sum of all bond energies associated with a single atom) of the surface Pt atoms.[27,29,30] Due to these factors, Pt(111) is the most desirable catalyst facet for many commercially as well as fundamentally important chemical transformations. For instance, recent theoretical investigations have shown that the Pt(111) plane is superior for the oxygen reduction reaction (ORR) due to a greater number of active sites for oxygen adsorption which leads to higher onset potential for O/OH adsorption and less surface poisoning.[8,13,31−33] In addition to single crystalline planes, the 111/111 edges having the highest coordination to the neighboring surface atoms also contribute to the ORR activities when compared with other edges.[28] This is because a higher coordination number leads to broadening of

Received: January 10, 2015
Accepted: February 6, 2015
Published: February 9, 2015

DOI: 10.1021/acsami.5b00211
ACS Appl. Mater. Interfaces 2015, 7, 4998−5005

d-band and higher d-band filling which in turn causes a weaker Pt−O bond at these sites.[34] Therefore, due to the largest number of exposed (111) atoms, Pt-NTds are preferred model systems for many industrial processes. To the best of our knowledge, however, there are only two methods to synthesize Pt-NTds in high-yield. El-Sayed and co-workers, in an early pioneering work, established the synthesis of ∼70% Pt-NTds using PVP and H_2.[35] Very recently, Chiu et al. showed that a suitable amino acid sequence can be designed to prepare ∼57% Pt-NTds.[36] Occasionally, however, mixtures of octahedral nanocrystals mixed with a smaller fraction of tetrahedral ones can be obtained.[11,37,38] Since the high yield methods use long surface stabilizing agents, their presence is expected to lead to deteriorated catalytic performance by interfering with the approach of the chemicals to the nanocrystal surface or by modifying the interactions of catalysts with its support, and therefore, additional surface treatment may be required to remove them.

Herein, we report a simple one-step and high-yield method to synthesize sub-10 nm Pt tetrahedral NCs, loaded onto a conducting carbon support (Pt-NTd/C) for electrocatalytic applications. No external reagent was used for controlling the selective growth of NC facets. Instead, a secondary amine species having a high affinity toward the closest-packed Pt(111) facets was generated in situ in the reaction. Dimethylamine so generated can be washed away from the catalyst surface, leading to bare Pt-NTd surfaces. External addition of secondary amine stabilizers results in much lower yields of Pt-NTds. The presence of carbon support in the reaction medium is crucial as it anchors the Pt nanoclusters generated at an early stage of the reaction and lets them evolve into shapes. The absence of carbon support encourages the association of NCs and formation of 1D nanowires by an oriented attachment mechanism. Due to the bare {111} facets, Pt-NTd/C exhibit excellent efficiency and stability toward the oxygen reduction reaction. We further report on the electrocatalytic oxidation efficiency of small renewable fuel molecules such as methanol and formic acid on the bare surfaces.

2. EXPERIMENTAL SECTION

Materials. Chloroplatinic acid ($H_2PtCl_6·6H_2O$, ≥37.50% Pt basis, Sigma-Aldrich), ethylene glycol (EG, 99%, SDFCL), *N*,*N*-dimethylformamide (DMF, 99.9%, Merck), amorphous carbon (Vulcan XC72), water (Millipore, 18.2 Ω), ethanol, and Nafion (5%, Sigma-Aldrich) were used without further purification.

Synthesis of Pt-NTd/C. 50 mg of H_2PtCl_6 was taken in a 25 mL round-bottom flask. Six mL of DMF and 4 mL of EG were added to dissolve the Pt precursor. 500 mg of KOH was added to the mixture and was stirred overnight at 27 °C. To the clear yellow colored solution so obtained, 14.2 mg of acid treated Vulcan-X72 carbon was added. The mixture was sonicated for 15 min and then was transferred into a 25 mL Teflon lined stainless steel autoclave. The autoclave was maintained at 170 °C for 8 h and then cooled to room temperature (it takes about 1.5 h for natural cooling). The black product so obtained was washed several times with water and ethanol and centrifuged at 10 000 rpm. The final product was then dispersed in ethanol and allowed to dry overnight at 70 °C in vacuum and used for various characterizations. To investigate the effect of various experimental parameters, control reactions were carried out with a different amount of solvents as well as using other relevant chemicals, as described in the text.

Synthesis of Pt Nanowire. The Pt nanowires (Pt-NW) were synthesized in a similar fashion (as described above) where the reaction was carried out in the absence of carbon support.

Functionalization of Carbon Support. One gram of carbon powder (Vulcan-X72) was exposed to 100 mL of 5 M HCl at 50 °C for 12 h with continuous stirring. This material (C_t) was washed with water and ethanol several times to remove excess HCl and dried at 60 °C in vacuum overnight. This treatment makes their dispersion extremely stable in polar solvents such as water (up to several hours). In addition, this treatment introduces surface functional groups, which is responsible for improved adsorption of metal salts.[39] This also leads to a high surface area of 497.8 m^2/g compared to 265.5 m^2/g for the untreated sample (see Figure S10, Supporting Information)

Control Experiments. In order to investigate *the effect of reaction time* on the evolution of the desired shape, reactions were carried out by varying the time of the solvothermal treatment (1, 2, 4, and 12h) and keeping all the other reaction conditions the same. In order to investigate the effect of solvent on shape of the NCs, reactions were performed by changing the relative ratios of DMF/EG systematically. For this, different amounts of DMF and EG were employed in the initial step of the reaction procedure. The various ratios of DMF/EG used were 0:10, 2:8, 4:6, 6:4, 8:2, and 10:0. In order to confirm the role of the secondary amine species in shape control, a reaction was carried out by replacing DMF with diethylamine and using EG as the only reducing agent.

Characterizations of Pt Nanocrystals. Powder X-ray diffraction data (PXRD) of all Pt-NTd/C catalysts were recorded using a Bruker AXS D8 Discover diffractometer attached with Cu Kα radiation. Field emission scanning electron microscopy (FESEM, FEI Quanta operated at 15 kV) and transmission electron microscopy (TEM, Technai F30 UHR, 200 kV, and FEI Titan 80−300 kV, aberration-corrected) were used to study the morphology and crystallinity of the Pt-NTd/C nanocrystals. X-ray photoelectron spectroscopy (XPS, VG Scientific ESCA LAB V) was employed to study the surface properties. The percentages of Pt loading on the carbon support were estimated by inductively coupled plasma optical emission spectroscopy (ICP-OES, Perkin−Elmer Optima 7000 DV). The ^1H nuclear magnetic resonance (NMR) measurements were carried out with NMR (Bruker AV-400) using a 10 μL aliquot in 0.5 mL of $CDCl_3$.

Electrochemical Investigations. The electrocatalytic activities of Pt-NTd/C, Pt-NW, and the commercial 40% Pt/C (Pt on graphitized carbon, Sigma-Aldrich) toward oxygen reduction reaction (ORR), methanol oxidation reaction (MOR), and formic acid oxidation (FAO) were studied by cyclic voltammetry (CV) and linear sweep voltammetry (LSV) techniques. The measurements were done on an electrochemical workstation (CHI760E and RRDE-3A) using a three electrode system: a glassy carbon (GC) electrode (3 mm in diameter) as substrate for working electrode, Ag/AgCl (3 M NaCl) as the reference electrode, and a platinum coil as the counter electrode. The measured potential with respect to the Ag/AgCl reference electrode were scaled to the reversible hydrogen electrode (RHE) by using the Nernst equation:

$$V(\mathrm{RHE}) = V(\mathrm{Ag/AgCl}) + V^{\circ}(\mathrm{Ag/AgCl}) + 0.059 \times \mathrm{pH} \quad (1)$$

For 0.1 M $HClO_4$, pH = 1 and V°(Ag/AgCl) (3 M NaCl) = 0.209 V at 25 °C.[40]

Prior to use, the GC electrode was well polished using alumina powders. Catalyst ink for the working electrode was prepared by dispersing 1.6 mg of Pt-NTd/C catalyst in 300 μL of nafion solution (5 wt % nafion/isopropanol/water = 0.05:1:4 (v/v/v)). Ten μL of this ink was drop-casted on the polished GC and allowed to dry. Pt loading on the GC was estimated to be 0.028 mg/cm^2. CV was recorded in Ar saturated 0.1 M $HClO_4$ (aq. solution) in the potential window of −0.25 to 0.9 V (vs. Ag/AgCl) at the scan rate of 50 mV/s.

The electrochemical active surface area of the Pt NS was calculated by the following relationship,

$$\mathrm{ECSA} = \frac{Q_{\mathrm{H}}}{q_{\mathrm{H}} \times (\mathrm{mg\,Pt})} \quad (2)$$

where q_H is the charge deposited per unit surface area of polycrystalline Pt electrode surface due to the underpotentially deposited monolayer of hydrogen atom on the Pt surface. q_H on 0.1

DOI: 10.1021/acsami.5b00211
ACS Appl. Mater. Interfaces 2015, 7, 4998−5005

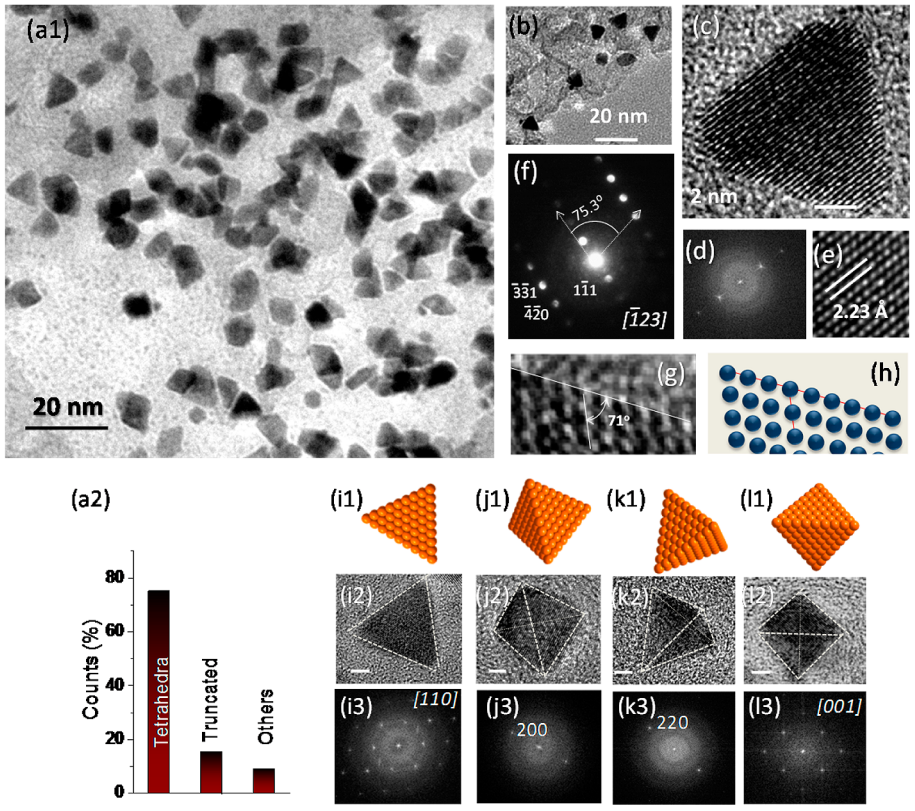

Figure 1. (a, b) TEM images of Pt-NTd/C obtained after 8 h using an EG/DMF ratio of 4:6. (a2) Shape distribution of the NCs. (c, d, e) HRTEM image and the corresponnding FT pattern of a Pt particle. (f) SAED pattern of the particle viewed along the [$\bar{1}$23] zone axis. (g) HRTEM image of an edge of a particle and (h) the corresponding model showing the atomic arrangement (i–l): (1) Atomic model, (2)TEM images, and (3) corresponding FFT patterns of various Pt-tetrahedron nanocrystals from different projections. The scale bars in the (i–l) TEM images denote 2 nm.

M $HClO_4$ is equal to 210 $\mu C/cm^2$. Q_H is associated with the hydrogen adsorption calculated from the recorded CV of the Pt.[41]

LSV was performed in O_2 saturated 0.1 M $HClO_4$ in the potential range of −0.25 to 0.9 V and scan rate of 5 mV/s. The stability tests were done by performing accelerated CV cycles. For the MOR and FAO study, CV profiles were recorded at the scan rate of 20 mV/s in Ar saturated 0.1 M $HClO_4$ + 1 M CH_3OH and 0.1 M $HClO_4$ + 1 M HCOOH, respectively. For MOR and FAO, stability was checked by chronoamperometry measurements.

3. RESULTS AND DISCUSSION

The tetrahedral NCs were synthesized solvothermally on a functionalized carbon support at 170 °C using $H_2PtCl_6{\cdot}6H_2O$. A mixture of ethylene glycol (EG) and dimethylformamide (DMF) with a ratio of 4:6 in the presence of KOH was used as the solvent as well as the reducing agent (see the Supporting Information for details). Figure 1a,b shows the overview transmission electron microscope (TEM) images of Pt-NTd/C obtained after a period of 8 h. The NCs are uniform, with an average size of 7.1 ± 0.9 nm, and well dispersed on the carbon support (Figure S1, Supporting Information). A careful analysis of the images suggests that about 75% of the NCs are tetrahedra, the rest consists of other shapes (Figure 1a2). The powder X-ray diffraction pattern of the Pt-NTd/C confirms that the as-prepared sample is exclusively composed of face-centered cubic Pt (JCPDS #65-2868, a = 3.706(1) Å) (Figure S2, Supporting Information).

A high resolution (HR) TEM image of a tetrahedron and its Fourier transform (FFT) pattern are shown in Figure 1c,d, respectively, showing a single-crystalline nature. The lattice fringes parallel to the edge measures 2.23 Å corresponding to Pt(111) planes (Figure 1e) indicating that the facets at the surface are also {111}. Triangular appearance can also arise due to plate-like triangular Pt NCs, covered with {111} and {100} facets, in which case the particle is associated with the stacking fault along the [111].[42,43] We therefore recorded a selected area electron diffraction (SAED) pattern from a number of triangular particles (Figure 1f). The absence of the forbidden 1/3{422} reflection in them confirmed the tetrahedron shape of the NCs. Some particles were oriented close to the [110] zone axis enabling visualization of Pt edge atoms at the junction of two {111} planes (Figure 1g), closely matching the atomic model in Figure 1h. To examine the shape of non-triangular particles, various tilting experiments were carried out during TEM imaging (Figure S3, Supporting Information). Models of Pt-NTds in different projections along with HRTEM images and FT pattern are shown in Figure 1i–l.

Examination of the chemical nature of Pt-NTds by X-ray photoelectron spectroscopy (XPS, Figure 2) revealed the presence of both Pt(0) and Pt(II) species. The strong doublet at 74.4 and 71.1 eV appears due to the $4f_{5/2}$ and $4f_{7/2}$ states of Pt(0), corresponding to ∼80 mass%. The peaks centered at 78 and 72 eV suggests the presence of Pt(II), possibly originating from surface Pt−O species or interaction of Pt NCs with the functional groups of the support. The Pt(0)/Pt(II) ratio is much higher than commercial Pt/C and other Pt NCs with {111} facets.[44,45]

Investigation of the Reaction Mechanism. We performed several control experiments to gain insight into the growth mechanism. The reaction proceeds with progressively slow kinetics until completion in 12 h. Pt contents on

DOI: 10.1021/acsami.5b00211
ACS Appl. Mater. Interfaces 2015, 7, 4998−5005

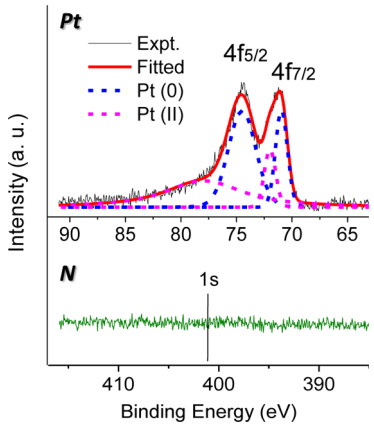

Figure 2. XPS spectra of Pt-NTd/C corresponding to Pt and N elements.

carbon support were estimated to be 9.7, 23, 28, and 30 wt % after 2, 4, 8, and 12 h of reaction time, respectively (Figure S4a, Supporting Information). The Pt-NTds appear as early as 1 h (Figures S4b and S5a, Supporting Information). In addition, the carbon support contained a large number of 2−4 nm Pt clusters initially (Figure S4c,d, Supporting Information), which disappeared after 4 h along with an increase in the number of NCs with tetrahedral morphology (Figure S5b, Supporting Information). With increasing reaction time, the Pt on the carbon support significantly increased in the early stage of the reaction, before slowing down.

In order to obtain the Pt-NTds, two factors were found to be crucial: (i) use of EG and DMF simultaneously in the reaction, which yields amine molecules in situ and (ii) the carbon support to arrest association of the incipient NTds. When the synthesis is carried out in EG or in DMF alone, the NCs develop irregular shapes (Figures 3a,b and S6, Supporting Information). On the other hand, using a mixture of DMF and EG in different proportions invariably led to Pt-NTd/C, though

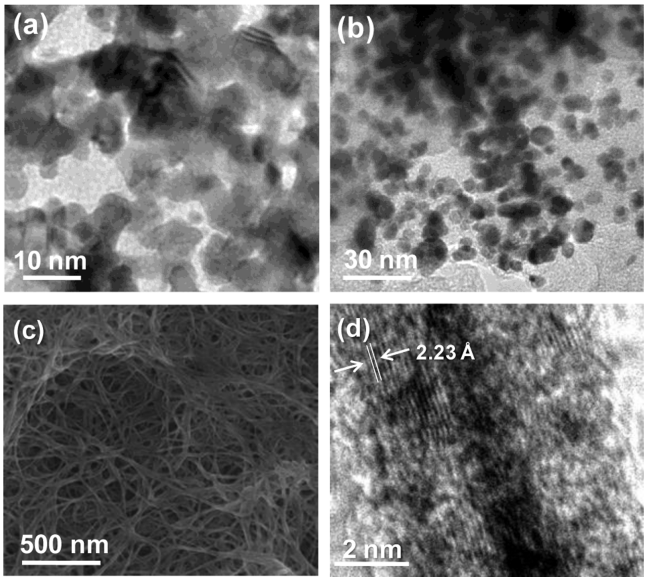

Figure 3. TEM images of NCs obtained using only (a) DMF or (b) EG at 170 °C. (c) FESEM image of the product obtained in the absence of carbon support in a similar experimental condition. (d) HRTEM image of a single nanowire.

yields are high only for certain solvent ratios. With increasing DMF fraction, the average size of the Pt-NTds increase initially reaching ∼9.7 nm, before reducing again (Figure S7, Supporting Information), also supported by XRD data (Figure S8, Supporting Information). For examining the role of carbon support, the synthesis was carried out without it, keeping the other parameters unaltered. This led to the formation of crystalline Pt nanowire bundles only (Figure 3c), and no particulates were found even in small numbers. Figure 3d is a high resolution TEM image of such a nanowire showing the lattice fringes of Pt(111) parallel to the nanowire wall. Similar results were observed in other studies as well.[45] On the basis of these observations, clearly, the DMF and EG mixture in the presence of KOH stabilizes the {111} planes of Pt. Usually, Pt(111) stabilization is achieved by using specific reagents such as PVP or peptide or by forming alloys.[25,35,36] Such stabilization depends not only upon the interaction strength of individual functional groups with the Pt surface but also on their packing efficiency on the Pt surface. This is probably the reason that different amine species were found to stabilize the {111} sub facets, Pt(X11), X = 3, 4, or 5 planes.[20] Theoretical investigations on the nature of interactions have shown that the stability of the NH species is more on Pt(111) than that of NH_2 on Pt(100).[46]

In our solvothermal conditions, a secondary amine is generated from the oxidation of DMF, as described below:

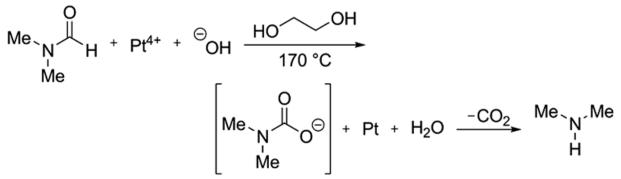

This was observed earlier in the case of reduction of Ag^+ salt.[47] Reduction of Pt^{4+} by DMF in the presence of KOH led to the formation of the carbamic acid intermediate which in the presence of protic solvent degrades to dimethylamine and CO_2 at high temperatures. Examination of our reaction mixture, which has a strong ammonia like pungent odor, was performed by nuclear magnetic resonance (NMR) spectroscopy (Figure 4a). A singlet peak at 2.33 ppm for two methyl ($-CH_3$) groups and multiplet at 0.843 ppm for N−H proton (the ratio of peak areas corresponding to the two methyl ($-CH_3$) groups to that for the N−H proton, I_{CH3}/I_{NH} = 5.908/1.056 = 5.6, ∼6) correspond to dimethylamine.[48] To be conclusive, we performed a control synthesis in the presence of diethylamine (DEA) using EG as solvent. The reaction product contained Pt-NTds anchored on carbon support as well as free-standing nanowires that arise due to solution phase nucleation and oriented attachment of NCs (Figures 4b,c and S10, Supporting Information). These observations confirm the role of amine and also point to the fact that in situ generation of amine is necessary for high yield generation of NTds. The activated carbon contains a high surface area and a large number of surface functional groups (Figure S11, Supporting Information). This increases the adsorption of Pt precursor and provides a large number of nucleation sites for growth of Pt-NTds.[49] We observed that, throughout the TEM grid, all Pt-NTds are attached to the carbon indicating that the NCs grew only on the support. We believe that, unlike the free-floating NCs solution, these anchored Pt-NTds cannot migrate and attach with each other to form nanowires by the oriented attachment mechanism.[45]

DOI: 10.1021/acsami.5b00211
ACS Appl. Mater. Interfaces 2015, 7, 4998−5005

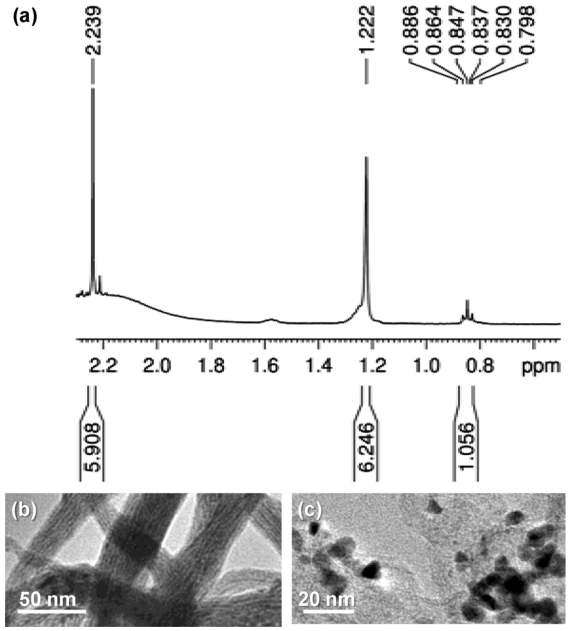

Figure 4. (a) NMR spectrum of the reaction mixture after an 8 h solvothermal treatment at 170 °C. (b, c) TEM images of products obtained from control experiments using only ethylene glycol as reducing agent in the presence of diethylamine. The formation of nanowire bundles along with tetrahedral morphology supports the stabilization of the Pt ⟨111⟩ plane by secondary amine species.

On the basis of these observations, we propose a growth mechanism for the Pt-NTd/C (Scheme 1). Nucleation of the

Scheme 1. Schematic Illustration of Synthesis of Pt-NTd/C

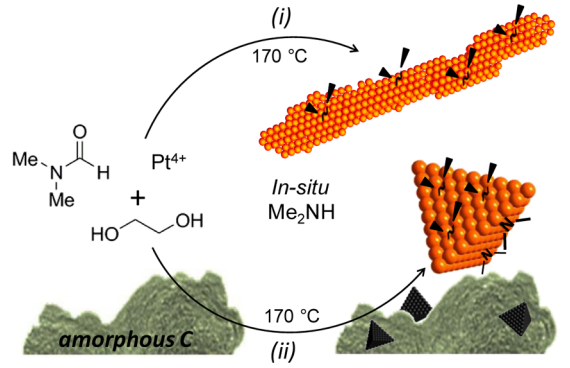

Pt-NTds first takes place in the carbon support. The in situ generated DMA stabilizes the Pt(111) facet, leading to formation of Pt tetrahedra NCs. Importantly, we found that the amine molecules can be easily removed from the Pt sample by repeated washing with a water/ethanol mixture (absence of nitrogen is seen in XPS spectra in Figure 2). Since DMA is the most strongly interacting molecule with Pt-NTds in the reaction mixture, its removal suggests that Pt(111) facets are free and exposed.

Electrocatalytic Performance of Bare Pt-NTds. The presence of strongly attached surface stabilizing agent may suppress the catalytic activity of nanoparticles of a noble metal, whose efficiencies are otherwise good.[50−52] Since, in our case, the surface stabilizing agents for the formation of Pt-NTd can be easily removed, the catalytic performance is expected to be high and true to the particular crystal-facet for electron transfer reactions. We have therefore examined the stability and activity of the Pt-NTds toward fuel cell reduction as well as oxidation reactions such as ORR, MOR, and FAO.

We investigated the long-term stability and electrocatalytic efficiency of the Pt-NTds using a three electrode system with Ag/AgCl (3 M NaCl) as reference electrode. Cyclic voltammograms (CV) were recorded with a sweep rate of 50 mV/s at 27 °C. For comparison, the performances of commercial carbon supported Pt NCs (C−Pt/C) were evaluated under identical conditions. Figure 5a shows CV plots for the Pt-NTd/C before

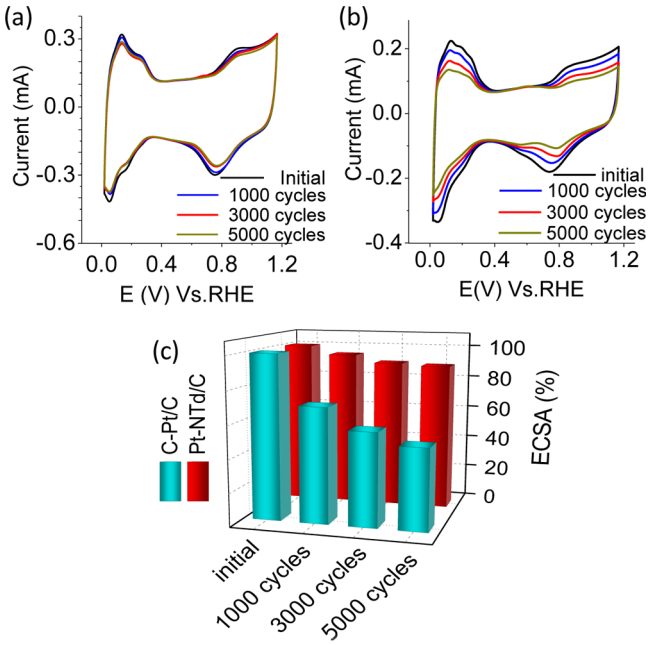

Figure 5. CV of (a) Pt-NTd/C and (b) commercial Pt/C before and after the stability test (in Ar saturated 0.1 M $HClO_4$ solution with 50 mV/s scan rate). (c) Surface areas of Pt-NTd/C (red) and C−Pt/C (cyan).

and after recycling for 1000, 3000, and 5000 cycles. It nearly maintained the distinct hydrogen adsorption/desorption peaks ($0.05 < V < 0.4$ V vs RHE) even after 5000 cycles, accompanied by a minimal decrease in the peak current. It is important to note that the distinct butterfly like shape of the CV is characteristic to the Pt(111) surface and further establishes our TEM observations.[32] C−Pt/C was distinctly different, as these peaks diminished quickly, exhibiting a gradual decrease in peak current (Figure 5b). The initial electrochemically active surface area (ECSA) for the Pt-NTd/C and C−Pt/C was comparable (19.22 and 17.62 m^2/g Pt, respectively). The ECSA for the Pt-NTd/C is maintained at ∼90% even after 5000 cycles. On the other hand, ECSA of the C−Pt/C reduced to 49.5% after 5000 cycles (Figure 5c). Their high durability, compared to many other shapes,[41,45,53] is due to structural stability due to higher cohesive energy of surface Pt atoms on {111} planes. Moreover, due to strong attachment to the carbon support, these NCs might avoid gradual agglomeration and Ostwald ripening.[41,54]

The ORR activities of the Pt-NTd/C were investigated by recording polarization curves and calculating the kinetic current densities using the Koutecký−Levich equation (Figures 6a and S12, Supporting Information).

DOI: 10.1021/acsami.5b00211
ACS Appl. Mater. Interfaces 2015, 7, 4998−5005

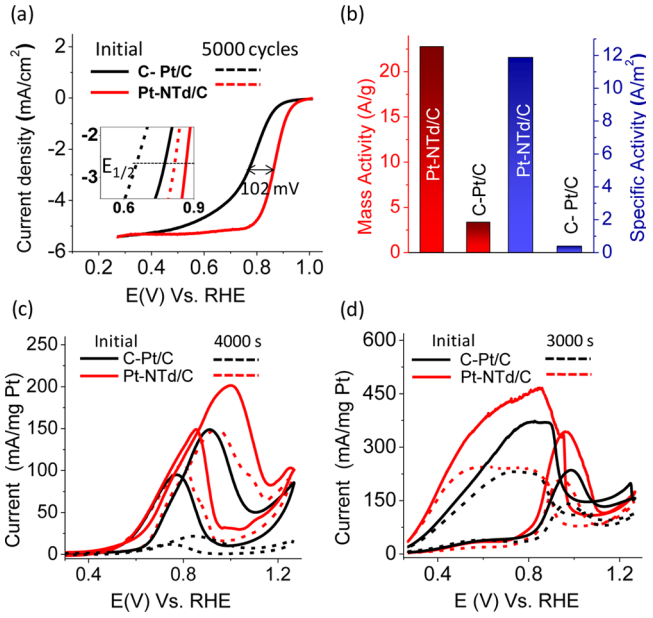

Figure 6. (a) LSV of Pt-NTd/C (red) and commercial Pt/C (black) in O_2 saturated 0.1 M $HClO_4$ with a scan rate 5 mV/s. Inset shows the change in $E_{1/2}$ after 5000 potential cycles for both the catalysts. (b) Comparison of mass and specific activitiesof Pt-NTd/C and the commercial one at 0.9 V. CV of Pt-NTd/C and commercial Pt/C before and after stability test for (c) MOR recorded in 0.1 M $HClO_4$ + 1 M CH_3OH and (d) FAO recorded in 0.1 M $HClO_4$ + 1 M HCOOH at scan rate 20 mV/s.

$$1/I = 1/I_k + 1/I_d \quad (3)$$

Here I, I_k, and I_d are measured, kinetic, and diffusion limited currents, respectively. The Pt-NTd/C exhibited a good onset potential of +1.011 V (vs RHE) as compared to +0.951 V recorded for the commercial catalyst. The corresponding half-wave potentials ($E_{1/2}$) show a significant positive shift of 102 mV (0.873 and 0.771 V for Pt-NTd/C and C−Pt/C, respectively) indicating much improved ORR kinetics. We also compared the ORR activities of the Pt nanowires obtained in absence of the carbon support. The nanowires exhibited an ORR onset and half-wave potential of +0.968 and +0.796 V, respectively (Figure S13, Supporting Information). Such superior ORR activity of Pt-NTd/C can be attributed to the presence of bare Pt ⟨111⟩ facets and 111/111 edges which allow easy electron transfer from catalyst to adsorbed oxygen[28] whereas in the case of Pt NW, along with exposure of Pt ⟨111⟩ facets in certain places, the oriented attachment mechanism may give rise to many defect sites giving rise to comparatively sluggish reduction kinetics. Furthermore, we compared the stability of the Pt-NTds with that for C−Pt/C. After 5000 cycles, the Pt-NTd/C showed nearly the same onset potential and a minimal 47 mV decrease in $E_{1/2}$. In comparison, C−Pt/C recorded a substantial decrease on onset and $E_{1/2}$ values by 130 mV, respectively (inset in Figure 6a). Mass activity of the Pt-NTd/C at 0.9 V (and at 0.85 V) is 22.8 A/g (104.6 A/g), which is 6.76 times higher than the C−Pt/C (Figures 6b and S12c, Supporting Information). Mass activity of the Pt-nanowires at 0.85 V was estimated to be 24.5 A/g (see Figure S13d, Supporting Information, for comparison of mass activities of all samples). The $E_{1/2}$ values recorded for these Pt-NTd/C are comparable to or better than most state of the art Pt electrocatalysts reported recently (Tables S1 and S2, Supporting Information).

We have further studied the electrochemical oxidation of small organic fuel molecules such as methanol and formic acid (MOR and FAO, respectively). The CV (Figure 6c) shows two distinct anodic current peaks typical of methanol oxidation in the forward and backward sweeps in the cyclic voltammogram. The corresponding mass and specific activities are compared with those of C−Pt/C in Figure S15a,b, Supporting Information. Initially, the mass and specific activities of Pt-NTd/C for MOR were 201.35 A/g and 23.56 A/m^2, respectively, much higher than 148.68 A/g and 8.38 A/m^2, respectively, recorded for C−Pt/C and comparable to most state of the art catalyst systems (Tables S3 and S4, Supporting Information). The ratio of the forward and backward peak current (I_f/I_b) measured 1.39 indicating high relative oxidation of fuel molecules in the forward scan as compared to many recently developed catalytic particles.[55−58] A new study by Tong and co-workers pointed out that oxidation of methanol takes place in both forward and reverse scans, contrary to a belief that the reverse peak is due to oxidation of residual carbon species.[59] We further examined the catalytic performance of these particles after 4000 s by employing chronoamperometry. Pt-NTd/C retained 52% of the initial activity, while the deactivation of C−Pt/C was far rapid.[49,55,60] Interestingly, in the case of FAO too, as during MOR, the I_f/I_b ratio for Pt-NTd/C was found to be very small (0.73) as compared to most other efficient Pt nanocrystals reported earlier (Figure 6d).[11,61,62] Pt-NTd/C has shown mass and specific activities of 312.65 A/g and 17.59 A/m^2, respectively, which decreased by 31% after 3000 s, whereas the corresponding activity loss for the C−Pt/C was recorded as 54% (Figure S15c,d, Supporting Information). In both cases, the high stability of Pt-NTd/C during the electrochemical process can be attributed to the highest cohesive energy of surface atoms on exposed Pt ⟨111⟩ planes giving rise to the lowest electrochemical leaching probability.[27] The ORR, MOR, and FAO studies clearly show that the Pt-NTds/C exhibit not only impressive electrocatalytic efficiency but also high stability under corrosive conditions.

4. CONCLUSION

We have synthesized sub-10 nm Pt tetrahedral NCs by a facile hydrothermal method, in the absence of any external stabilizing agents. We establish that amine species generated in situ from the reaction of EG and DMF in the presence of KOH at elevated tempeature and the nucleation induced by the carbon support is responsible for generating such shape. The role of the carbon support is crucial in this synthesis as it anchors the Pt NTds during the nucleation and growth stages, thereby inhibiting the possibility of nanowire formation by the easy association of the bare NCs. The Pt(111) stabilizer, dimethylamine, can be easily removed from the NC surface, leaving its surface entirely exposed. We found that these Pt-NTd/C exhibit excellent stability (~90% activity retention) as compared to the commercially available electrocatalysts under harsh reaction conditions. Furthermore, our sample exhibited superior electrocatalytic efficiencies toward both fuel cell oxidation and reduction reactions. The onset potential of 1.01 V for ORR is higher than other known carbon supported Pt NCs. With the bare nature of Pt(111) surfaces, our Pt-NTd/C not only are promising for fuel cell applications but also may

DOI: 10.1021/acsami.5b00211
ACS Appl. Mater. Interfaces 2015, 7, 4998−5005

be excellent model catalysts for many other important catalytic reactions.

■ ASSOCIATED CONTENT

Supporting Information

Detailed description of the experimental procedure, additional SEM, TEM analysis, XRD, XPS, BET, CVs, LSV, KL plots, and comparison of catalytic activities. This material is available free of charge via the Internet at http://pubs.acs.org.

■ AUTHOR INFORMATION

Corresponding Author

*E-mail: ujjalgautam@gmail.com.

Author Contributions

‡M.R. and M.C. contributed equally.

Notes

The authors declare no competing financial interest.

■ ACKNOWLEDGMENTS

The authors thank Prof. CNR Rao, FRS, for his constant inspiration and advanced electron microscopy facilities. M.R. thanks CSIR (India) for SRF. M.C. thanks UGC (India) for JRF. U.K.G. thanks DST (India) for the Ramanujan Fellowship and Sheikh Saqr Laboratory for research funding.

■ REFERENCES

(1) Mahmoud, M. A.; Narayanan, R.; El-Sayed, M. A. Enhancing Colloidal Metallic Nanocatalysis: Sharp Edges and Corners for Solid Nanoparticles and Cage Effect for Hollow Ones. *Acc. Chem. Res.* **2013**, *46*, 1795−1805.

(2) Kang, Y.; Pyo, J. B.; Ye, X.; Diaz, R. E.; Gordon, T. R.; Stach, E. A.; Murray, C. B. Shape-Controlled Synthesis of Pt Nanocrystals: The Role of Metal Carbonyls. *ACS Nano* **2013**, *7*, 645−653.

(3) Guo, S.; Zhang, S.; Sun, S. Tuning Nanoparticle Catalysis for the Oxygen Reduction Reaction. *Angew. Chem., Int. Ed.* **2013**, *52*, 8526−8544.

(4) Chen, J. S.; Zhu, T.; Hu, Q. H.; Gao, J.; Su, F.; Qiao, S. Z.; Lou, X. W. Shape-Controlled Synthesis of Cobalt-Based Nanocubes, Nanodiscs, and Nanoflowers and Their Comparative Lithium-Storage Properties. *ACS Appl. Mater. Interfaces* **2010**, *2*, 3628−3635.

(5) Wang, D.-Y.; Chou, H.-L.; Cheng, C.-C.; Wu, Y.-H.; Tsai, C.-M.; Lin, H.-Y.; Wang, Y.-L.; Hwang, B.-J.; Chen, C.-C. FePt Nanodendrites with High-Index Facets As Active Electrocatalysts for Oxygen Reduction Reaction. *Nano Energy* **2015**, *11*, 631−639.

(6) Lee, I.; Morales, R.; Albiter, M. A.; Zaera, F. Synthesis of Heterogeneous Catalysts with Well Shaped Platinum Particles to Control Reaction Selectivity. *Proc. Natl. Acad. Sci. U. S. A.* **2008**, *105*, 15241−15246.

(7) Lee, I.; Delbecq, F.; Morales, R.; Albiter, M. A.; Zaera, F. Tuning Selectivity in Catalysis by Controlling Particle Shape. *Nat. Mater.* **2009**, *8*, 132−138.

(8) Nørskov, J. K.; Rossmeisl, J.; Logadottir, A.; Lindqvist, L.; Kitchin, J. R.; Bligaard, T.; Jónsson, H. Origin of the Overpotential for Oxygen Reduction at a Fuel-Cell Cathode. *J. Phys. Chem. B* **2004**, *108*, 17886−17892.

(9) Kang, Y.; Li, M.; Cai, Y.; Cargnello, M.; Diaz, R. E.; Gordon, T. R.; Wieder, N. L.; Adzic, R. R.; Gorte, R. J.; Stach, E. A.; Murray, C. B. Heterogeneous Catalysts Need Not Be so "Heterogeneous": Monodisperse Pt Nanocrystals by Combining Shape-Controlled Synthesis and Purification by Colloidal Recrystallization. *J. Am. Chem. Soc.* **2013**, *135*, 2741−2747.

(10) Li, C.; Jiang, B.; Imura, M.; Malgras, V.; Yamauchi, Y. Mesoporous Pt Hollow Cubes with Controlled Shell Thicknesses and Investigation of Their Electrocatalytic Performance. *Chem. Commun.* **2014**, *50*, 15337−15340.

(11) Solla-Gullon, J.; Vidal-Iglesias, F. J.; Lopez-Cudero, A.; Garnier, E.; Feliu, J. M.; Aldaz, A. Shape-Dependent Electrocatalysis: Methanol and Formic Acid Electrooxidation on Preferentially Oriented Pt Nanoparticles. *Phys. Chem. Chem. Phys.* **2008**, *10*, 3689−3698.

(12) Xia, Y.; Xiong, Y.; Lim, B.; Skrabalak, S. E. Shape-Controlled Synthesis of Metal Nanocrystals: Simple Chemistry Meets Complex Physics? *Angew. Chem., Int. Ed.* **2009**, *48*, 60−103.

(13) Du, L.; Zhang, S.; Chen, G.; Yin, G.; Du, C.; Tan, Q.; Sun, Y.; Qu, Y.; Gao, Y. Polyelectrolyte Assisted Synthesis and Enhanced Oxygen Reduction Activity of Pt Nanocrystals with Controllable Shape and Size. *ACS Appl. Mater. Interfaces* **2014**, *6*, 14043−14049.

(14) Ouyang, J.; Pei, J.; Kuang, Q.; Xie, Z.; Zheng, L. Supersaturation-Controlled Shape Evolution of α-Fe_2O_3 Nanocrystals and Their Facet-Dependent Catalytic and Sensing Properties. *ACS Appl. Mater. Interfaces* **2014**, *6*, 12505−12514.

(15) Koenigsmann, C.; Wong, S. S. One-Dimensional Noble Metal Electrocatalysts: A Promising Structural Paradigm for Direct Methanol Fuel Cells. *Energy Environ. Sci.* **2011**, *4*, 1161−1176.

(16) Gan, L.; Cui, C.; Heggen, M.; Dionigi, F.; Rudi, S.; Strasser, P. Element-Specific Anisotropic Growth of Shaped Platinum Alloy Nanocrystals. *Science* **2014**, *346*, 1502−1506.

(17) Wang, C.; Daimon, H.; Lee, Y.; Kim, J.; Sun, S. Synthesis of Monodisperse Pt Nanocubes and Their Enhanced Catalysis for Oxygen Reduction. *J. Am. Chem. Soc.* **2007**, *129*, 6974−6975.

(18) Tian, N.; Zhou, Z.-Y.; Sun, S.-G.; Ding, Y.; Wang, Z. L. Synthesis of Tetrahexahedral Platinum Nanocrystals with High-Index Facets and High Electro-Oxidation Activity. *Science* **2007**, *316*, 732−735.

(19) Wang, L.; Wang, H.; Nemoto, Y.; Yamauchi, Y. Rapid and Efficient Synthesis of Platinum Nanodendrites with High Surface Area by Chemical Reduction with Formic Acid. *Chem. Mater.* **2010**, *22*, 2835−2841.

(20) Huang, X.; Zhao, Z.; Fan, J.; Tan, Y.; Zheng, N. Amine-Assisted Synthesis of Concave Polyhedral Platinum Nanocrystals Having {411} High-Index Facets. *J. Am. Chem. Soc.* **2011**, *133*, 4718−4721.

(21) Koenigsmann, C.; Scofield, M. E.; Liu, H.; Wong, S. S. Designing Enhanced One-Dimensional Electrocatalysts for the Oxygen Reduction Reaction: Probing Size- and Composition-Dependent Electrocatalytic Behavior in Noble Metal Nanowires. *J. Phys. Chem. Lett.* **2012**, *3*, 3385−3398.

(22) Wang, Y.; Xie, S.; Liu, J.; Park, J.; Huang, C. Z.; Xia, Y. Shape-Controlled Synthesis of Palladium Nanocrystals: A Mechanistic Understanding of the Evolution from Octahedrons to Tetrahedrons. *Nano Lett.* **2013**, *13*, 2276−2281.

(23) Wang, Z. L.; Petroski, J. M.; Green, T. C.; El-Sayed, M. A. Shape Transformation and Surface Melting of Cubic and Tetrahedral Platinum Nanocrystals. *J. Phys. Chem. B* **1998**, *102*, 6145−6151.

(24) Peng, Z.; Yang, H. Designer Platinum Nanoparticles: Control of Shape, Composition in Alloy, Nanostructure and Electrocatalytic Property. *Nano Today* **2009**, *4*, 143−164.

(25) Chen, M.; Wu, B.; Yang, J.; Zheng, N. Small Adsorbate-Assisted Shape Control of Pd and Pt Nanocrystals. *Adv. Mater.* **2012**, *24*, 862−879.

(26) Yin, A.-X.; Min, X.-Q.; Zhang, Y.-W.; Yan, C.-H. Shape-Selective Synthesis and Facet-Dependent Enhanced Electrocatalytic Activity and Durability of Monodisperse Sub-10 nm Pt-Pd Tetrahedrons and Cubes. *J. Am. Chem. Soc.* **2011**, *133*, 3816−3819.

(27) Lu, H. M.; Meng, X. K. Theoretical Model to Calculate Catalytic Activation Energies of Platinum Nanoparticles of Different Sizes and Shapes. *J. Phys. Chem. B* **2009**, *114*, 1534−1538.

(28) Shao, M.; Peles, A.; Shoemaker, K. Electrocatalysis on Platinum Nanoparticles: Particle Size Effect on Oxygen Reduction Reaction Activity. *Nano Lett.* **2011**, *11*, 3714−3719.

(29) Jiang, Q.; Li, J. C.; Chi, B. Q. Size-Dependent Cohesive Energy of Nanocrystals. *Chem. Phys. Lett.* **2002**, *366*, 551−554.

(30) Chepulskii, R. V.; Curtarolo, S. Ab Initio Insights on the Shapes of Platinum Nanocatalysts. *ACS Nano* **2010**, *5*, 247−254.

(31) Tripković, V.; Cerri, I.; Bligaard, T.; Rossmeisl, J. The Influence of Particle Shape and Size on the Activity of Platinum Nanoparticles

DOI: 10.1021/acsami.5b00211
ACS Appl. Mater. Interfaces 2015, 7, 4998−5005

for Oxygen Reduction Reaction: A Density Functional Theory Study. *Catal. Lett.* **2014**, *144*, 380−388.
(32) Koenigsmann, C.; Zhou, W.-p.; Adzic, R. R.; Sutter, E.; Wong, S. S. Size-Dependent Enhancement of Electrocatalytic Performance in Relatively Defect-Free, Processed Ultrathin Platinum Nanowires. *Nano Lett.* **2010**, *10*, 2806−2811.
(33) Subhramannia, M.; Pillai, V. K. Shape-Dependent Electrocatalytic Activity of Platinum Nanostructures. *J. Mater. Chem.* **2008**, *18*, 5858−5870.
(34) Hammer, B.; Nørskov, J. Electronic Factors Determining the Reactivity of Metal Surfaces. *Surf. Sci.* **1995**, *343*, 211−220.
(35) Ahmadi, T. S.; Wang, Z. L.; Green, T. C.; Henglein, A.; El-Sayed, M. A. Shape-Controlled Synthesis of Colloidal Platinum Nanoparticles. *Science* **1996**, *272*, 1924−1925.
(36) Chiu, C.-Y.; Li, Y.; Ruan, L.; Ye, X.; Murray, C. B.; Huang, Y. Platinum Nanocrystals Selectively Shaped Using Facet-Specific Peptide Sequences. *Nat. Chem.* **2011**, *3*, 393−399.
(37) Levendorf, A. M.; Chen, D.-J.; Rom, C. L.; Liu, Y.; Tong, Y. J. Electrochemical and in Situ ATR-SEIRAS Investigations of Methanol and CO Electro-Oxidation on PVP-Free Cubic and Octahedral/Tetrahedral Pt Nanoparticles. *RSC Adv.* **2014**, *4*, 21284−21293.
(38) Song, H.; Kim, F.; Connor, S.; Somorjai, G. A.; Yang, P. Pt Nanocrystals: Shape Control and Langmuir-Blodgett Monolayer Formation. *J. Phys. Chem. B* **2005**, *109*, 188−193.
(39) Ye, J.; Liu, J.; Zhou, Y.; Zou, Z.; Gu, J.; Yu, T. High Catalytic Performance and Stability of Pt/C Using Acetic Acid Functionalized Carbon. *J. Power Sources* **2009**, *194*, 683−689.
(40) Tong, L.; Iwase, A.; Nattestad, A.; Bach, U.; Weidelener, M.; Gotz, G.; Mishra, A.; Bauerle, P.; Amal, R.; Wallace, G. G.; Mozer, A. J. Sustained Solar Hydrogen Generation Using a Dye-Sensitised NiO Photocathode/BiVO4 Tandem Photo-Electrochemical Device. *Energy Environ. Sci.* **2012**, *5*, 9472−9475.
(41) Sun, S.; Zhang, G.; Geng, D.; Chen, Y.; Li, R.; Cai, M.; Sun, X. A Highly Durable Platinum Nanocatalyst for Proton Exchange Membrane Fuel Cells: Multiarmed Starlike Nanowire Single Crystal. *Angew. Chem., Int. Ed.* **2011**, *50*, 422−426.
(42) Wang, Z. L. Transmission Electron Microscopy of Shape-Controlled Nanocrystals and Their Assemblies. *J. Phys. Chem. B* **2000**, *104*, 1153−1175.
(43) Xiong, Y.; Washio, I.; Chen, J.; Cai, H.; Li, Z.-Y.; Xia, Y. Poly(vinyl pyrrolidone): A Dual Functional Reductant and Stabilizer for the Facile Synthesis of Noble Metal Nanoplates in Aqueous Solutions. *Langmuir* **2006**, *22*, 8563−8570.
(44) Tian, Z. Q.; Jiang, S. P.; Liang, Y. M.; Shen, P. K. Synthesis and Characterization of Platinum Catalysts on Multiwalled Carbon Nanotubes by Intermittent Microwave Irradiation for Fuel Cell Applications. *J. Phys. Chem. B* **2006**, *110*, 5343−5350.
(45) Xia, B. Y.; Wu, H. B.; Yan, Y.; Lou, X. W.; Wang, X. Ultrathin and Ultralong Single-Crystal Platinum Nanowire Assemblies with Highly Stable Electrocatalytic Activity. *J. Am. Chem. Soc.* **2013**, *135*, 9480−9485.
(46) Novell-Leruth, G.; Valcárcel, A.; Clotet, A.; Ricart, J. M.; Pérez-Ramírez, J. DFT Characterization of Adsorbed NHx Species on Pt(100) and Pt(111) Surfaces. *J. Phys. Chem. B* **2005**, *109*, 18061−18069.
(47) Pastoriza-Santos, I.; Liz-Marzán, L. M. Reduction of Silver Nanoparticles in DMF. Formation of Monolayers and Stable Colloids. *Pure Appl. Chem.* **2000**, *72*, 83−90.
(48) Abraham, R. J.; Byrne, J. J.; Griffiths, L.; Perez, M. 1H Chemical Shifts in NMR: Part 23, the Effect of Dimethyl Sulfoxide versus Chloroform Solvent on 1H Chemical Shifts. *Magn. Reson. Chem.* **2006**, *44*, 491−509.
(49) Kundu, P.; Nethravathi, C.; Deshpande, P. A.; Rajamathi, M.; Madras, G.; Ravishankar, N. Ultrafast Microwave-Assisted Route to Surfactant-Free Ultrafine Pt Nanoparticles on Graphene: Synergistic Co-reduction Mechanism and High Catalytic Activity. *Chem. Mater.* **2011**, *23*, 2772−2780.
(50) Ye, H.; Crooks, R. M. Electrocatalytic O_2 Reduction at Glassy Carbon Electrodes Modified with Dendrimer-Encapsulated Pt Nanoparticles. *J. Am. Chem. Soc.* **2005**, *127*, 4930−4934.
(51) Gong, K.; Vukmirovic, M. B.; Ma, C.; Zhu, Y.; Adzic, R. R. Synthesis and Catalytic Activity of Pt Monolayer on Pd Tetrahedral Nanocrystals with CO-Adsorption-Induced Removal of Surfactants. *J. Electroanal. Chem.* **2011**, *662*, 213−218.
(52) Lei, M.; Liang, C.; Huan, Q.; Miyabayashi, K.; Miyake, M.; Yang, T. Morphology-Controlled Growth of Pt Nanoparticles Taking Advantage of Smaller Molecule and Inorganic Salt. *Acta Mater.* **2014**, *63*, 202−208.
(53) Narayanamoorthy, B.; Datta, K. K. R.; Eswaramoorthy, M.; Balaji, S. Improved Oxygen Reduction Reaction Catalyzed by Pt/Clay/Nafion Nanocomposite for PEM Fuel Cells. *ACS Appl. Mater. Interfaces* **2012**, *4*, 3620−3626.
(54) Ferreira, P. J.; Shao-Horn, Y.; Morgan, D.; Makharia, R.; Kocha, S.; Gasteiger, H. A. Instability of Pt/C Electrocatalysts in Proton Exchange Membrane Fuel Cells a Mechanistic Investigation. *J. Electrochem. Soc.* **2005**, *152*, A2256−A2271.
(55) Li, C.; Sato, T.; Yamauchi, Y. Electrochemical Synthesis of One-Dimensional Mesoporous Pt Nanorods Using the Assembly of Surfactant Micelles in Confined Space. *Angew. Chem., Int. Ed.* **2013**, *52*, 8050−8053.
(56) Li, C.; Yamauchi, Y. Facile Solution Synthesis of Ag@ Pt Core-Shell Nanoparticles with Dendritic Pt Shells. *Phys. Chem. Chem. Phys.* **2013**, *15*, 3490−3496.
(57) Bai, L.; Zhu, H.; Thrasher, J. S.; Street, S. C. Synthesis and Electrocatalytic Activity of Photoreduced Platinum Nanoparticles in a Poly(ethylenimine) Matrix. *ACS Appl. Mater. Interfaces* **2009**, *1*, 2304−2311.
(58) Koenigsmann, C.; Semple, D. B.; Sutter, E.; Tobierre, S. E.; Wong, S. S. Ambient Synthesis of High-Quality Ruthenium Nanowires and the Morphology-Dependent Electrocatalytic Performance of Platinum-Decorated Ruthenium Nanowires and Nanoparticles in the Methanol Oxidation Reaction. *ACS Appl. Mater. Interfaces* **2013**, *5*, 5518−5530.
(59) Hofstead-Duffy, A. M.; Chen, D.-J.; Sun, S.-G.; Tong, Y. J. Origin of the Current Peak of Negative Scan in the Cyclic Voltammetry of Methanol Electro-Oxidation on Pt-Based Electrocatalysts: A Revisit to the Current Ratio Criterion. *J. Mater. Chem.* **2012**, *22*, 5205−5208.
(60) Li, T.; You, H.; Xu, M.; Song, X.; Fang, J. Electrocatalytic Properties of Hollow Coral-like Platinum Mesocrystals. *ACS Appl. Mater. Interfaces* **2012**, *4*, 6942−6948.
(61) Kim, Y.; Kim, H. J.; Kim, Y. S.; Choi, S. M.; Seo, M. H.; Kim, W. B. Shape- and Composition-Sensitive Activity of Pt and PtAu Catalysts for Formic Acid Electrooxidation. *J. Phys. Chem. C* **2012**, *116*, 18093−18100.
(62) McCurry, D. A.; Kamundi, M.; Fayette, M.; Wafula, F.; Dimitrov, N. All Electrochemical Fabrication of a Platinized Nanoporous Au Thin-Film Catalyst. *ACS Appl. Mater. Interfaces* **2011**, *3*, 4459−4468.

DOI: 10.1021/acsami.5b00211
ACS Appl. Mater. Interfaces 2015, 7, 4998−5005